Design and Analysis of Force Feedback in Telerobotics

Mayez A. Al-Mouhamed[1], Mohammad Nazeeruddin[2], and Nesar Merah[3]

(1) Department of Computer Engineering

mayez@ccse.kfupm.edu.sa

(2) Department of Systems Engineering

nazeer@ccse.kfupm.edu.sa

(3) Department of Mechanical Engineering

nesar@kfupm.edu.sa

King Fahd University of Petroleum and Minerals (KFUPM)

Dhahran 31261, Saudi Arabia.

Abstract— **Telerobotics aims at extending eye-hand motion coordination through a computer network while preserving human dexterity. In this paper we present the design and analysis of force feedback in an Internet-based telerobotics. A master arm station (client) is connected to a slave arm station (server) using a distributed-component software system. The two stations exchanges (real-time) motion commands, force feedback, and stereo video information. To provide the operator with a feeling of the force applied on the remote tool a compliant force sensor is proposed. A six dof, parallel mechanism, wrist force sensor is described. The objective is to capture the force, relay the information over the Internet, and to display it on the operator using the master arm. Analysis of sensor kinematics aims at converting measured tip forces and torques into forces applied on the tool. Interaction and force feedback generated during contact with a rigid object, an elastic object, and a tissue are presented. Bouncing oscillations are observed in pre-contact phases depending on the force feedback gain. Analysis shows that teleoperation network delays and mechanism transmission elasticities contribute to system instability. Modeling of the interaction for the manipulated object should also be used to provide better teleoperation stability.**

Keywords: force feedback, force sensor, man-machine interface, Telerobotics.

I. INTRODUCTION

Telerobotics aims at extending the human natural eye-hand motion coordination over an arbitrary distance and an arbitrary scale. The objective is to replicate human skills and dexterity to a remote work place. Human psychomotor skills have evolved over billion of years which explain the difficulty in designing a high-fidelity telepresence system. Timely interacting with the environment using visual, haptic, and force feedbacks are required. The two major limiting factors are the lack of an effective man-machine interfacing and the transmission delays.

Parallel actuation in teleoperation [1], [2] uses a coarse-fine slave arm with a fine-motion wrist identical to the master arm. Fine motion is based on Lorentz magnetic levitation. The wrist-level coordinated force provides a transparent and massless rigid mapping, uncoupled coarse-fine control, and high-performance in free-motion tracking as well as in contact tasks.

A miniature force sensor [3] measures contact forces at the tip of a microsurgical instrument for a cooperatively manipulated microsurgical assistant. Position-controlled motion with micrometer resolution is achieved. Reaction to less than 5 mN is reported. However, large force errors were reported when force sensor tip velocity was high which is not the case in microsurgery.

To reduce the operating load such as end-effector, payload, gravity, and damping cause by force feedback a Cartesian mapping [4] is proposed instead of a joint-to- mapping. This allows carrying out a task wrench with reduced contact wrenches. The method is also useful for kinesthetic haptic display in virtual or simulated environments. The remotely-sensed task wrench or computer generated virtual task wrench can be sent to the active hand controller to let the user feels the tasks wrench. The hand controller has man-machine has bottoms for (1) wrench reflection mapping, (2) force reflecting reference pose and indexing, and (3) wrench reflection. Wrench-reflection to the operator promotes lower contact wrenches. The amount of work in peg-in-hole insertion is reduced to about one third than without force information.

A micro/nano space is operated using a task-oriented teleoperation system [5]. A mixed of direct and task oriented modes are activated using a set of visualization and manipulation tools with some force monitoring. To avoid collision high-level motion commands are used. The approach is faster and safer with higher accuracy than direct teleoperation given the presence of dominant electrostatic forces and possible sticking of handling tool.

A six-axis force reflective hand controller (FRHC) is evaluated using kinesthetic and stereo video HMD [4]. The operator position is mapped to slave arm both is position and velocity. Evaluation of a drill task indicates equal task times but with noticeably lower cumulative, variances, and peak forces when either visual or kinesthetic force is used with stereo vision (HMD). Force feedback is particularly useful in the case of unobstructed camera view leading to a low fidelity stereo video.

supervisory control is also useful to overcome communication delays and reliability and the need to failure recovery and

safe system operations [6].

A telerobotic framework is evaluated using direct teleoperation with the following schemes: (1) stereo vision, (2) vision and force feedback, and (3) vision with active compliance. Space indexing and scalability tools are also used. The above system is experimented using the following tasks (1) pouring of water, (2) peg-in-hole insertion, (3) assembly of a small water pump, (4) operating drawers, and (5) wire-wrapping. A motion mapping scheme is used to map operator hand motion to remote tool both in position and force. Strategy for task effective execution is presented for each of the above tasks. Analysis of task time, peak and average contact forces is presented together with remote operator interaction. Comments on the performance of each scheme as presented and compared to the others.

The organization of this paper is as follows. In Section II an overview of the telerobotic system architecture is presented. In Section III the force sensor kinematics is presented. In Section IV the evaluation is presented. We conclude in Section V.

II. TELEROBOTIC SYSTEM ARCHITECTURE

The aim is to extend natural eye-hand motion coordination through a computer network while preserving human manipulative dexterity in scaled working environments. The objective is to develop a multi-disciplinary telerobotic research environment integrating motion, vision, and haptic senses to experience telerobotic system interactions, man-machine interfacing, and computer aided teleoperation (CAT). For this an electro-mechanical system is developed as a client and server stations which are interconnected by a computer network integrating bilateral motion, stereo vision, and force feedback as well as some CAT tools.

A *Multi-Threaded Distributed Framework* (MTDF) [7] has been proposed based on an object-oriented client-server distributed component architecture with .NET remoting as a tool to provide object interactions through the Internet. A schematic of our telerobotic system is shown on Figure 1. The server station has (1) a slave arm module that consists of a PUMA (S_{PUMA}) and a Force (S_F) components, and (2) a video (S_V) component. The client station has (1) a master arm component that consists of a Motion (C_M) and a Force (C_F) processes, and (2) a video component (C_V). The multi-threaded aspects stem from the simultaneous activation of client and server threads. All client (server) components are concurrently run as independent threads on the client (server) computer. Real-time thread S_V (S_F, C_M) is logically interconnected to C_V (C_F, S_{PUMA}) to which it sends data through the network. Each component has layered structure starting from a physical level to an abstract information mapping level.

The following is a short description of thread function:

1) C_M regularly samples the master arm, computes variation in operator hand position using forward arm kinematics, and transfers position variation to S_{PUMA}.
2) S_{PUMA} receives variation in operator position, modifies slave arm tool position using inverse arm kinematics, and commands the slave motion accordingly.
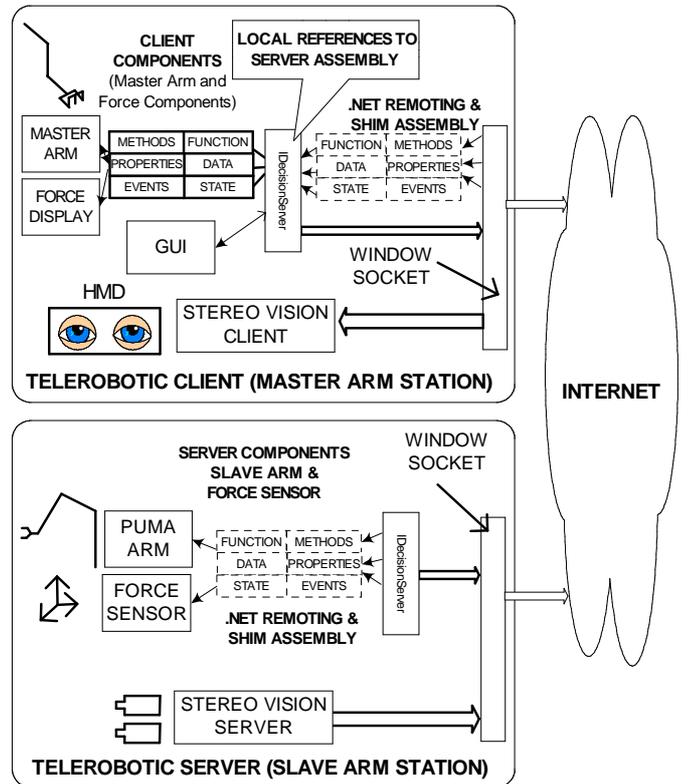
Fig. 1. Real-time transfer of motion command, force data, and live stereo video.

3) S_F regularly samples a wrist force sensor, evaluates force applied to tool, and streams computed force to C_F.
4) C_F receives force data, applies it to master arm tool using arm jacobian, and displays force.
5) S_V grabs two video images from cameras, and transfer them to C_V.
6) C_V receives a stereo image and display its 3D visualization.

The MTDF is based on the implementation of a client and a server components that are reliably connected by stereo, force, and commands data transfers through a network. The distributed approach leads the logic of the system be distributed in different software components. In the following we present the implementation of each of the client and server sub-systems.

The operator uses a light, 6 DOF, wire-based, anthropomorphic, master arm that was designed in our Robotics Lab at KFUPM. Some of the CAT functions can be activated using buttons disposed on the master arm handle. The CAT functions are (1) arm indexing, (2) space scalability, (3) tool frame definition, and (4) selection of motion mapping. Motion mapping refer to the mapping of operator hand motion to a specific frame of the slave arm, i.e. world, wrist, or tool frame. The user hand motion is mapped to a defaults too frame. In other words, the sensed force at the slave arm is computed with respect to the current tool frame before being transmitted to client station and displayed on the user hand. The above client and server setting are valid for all the experiments described in this part.

(a) The top and bottom disks are interconnected by using three rubber blocks

(b) Each rubber block has a pair of sensors, each sensor iconsists of an LED and a PT.

(c) Each left sensor measures horizontal displacements of the wing regardless of possible shifts in the vertical direction.

(d) Each right sensor measures vertical displacements of the wing regardless of possible shifts in the horizontal direction.

Fig. 2. Some details of the compliant force sensor

The master arm is used to display on the user a stream of reflected force feedback originated from the slave arm tool frame. In addition the user wears a head-mounted display (HMD) that receives live stereo video frames (17 stereo fps) originated from two cameras pointing to the workspace at the slave station. More information on performance can be found in [8].

III. WRIST FORCE SENSOR

A wrist force sensor is useful to provide both mechanical and electrical compliance at the tip of the slave robot arm. The electrical compliance or active compliance can be programmed to control the behavior of the slave arm in the presence of external forces. Its reaction depends on the activation of its control program. The presence of some mechanical compliance at the tip of the slave arm increases system reliability in assembly operations involving contact forces with unknown positioning. These conditions are present in most telerobotic operations involving object manipulation. In the following we present the design of compliant force sensor for teleoperation.

The force sensor (FS) is wrist device that consists two solid aluminum disks each is 60 mm in diameter and 3 mm in thickness as shown in Figure 2-(a). The two disks are interconnected by means of three parallel cube-shaped rubber blocks (10 mm^3) which are distributed along the three directions (120 degrees) to exhibit equal elasticity in all directions. Figure 2-(b) shows the two sensors placed at both sides of each block which measure orthogonal displacements caused by an external force or moment applied on the top disk (gripper), i.e. position and orientation displacement of gripper compared to arm wrist. Each sensor consists of an LED that generates a circular beam (3 mm diameter) of red

light in front of a photo-transistor (PT). Both LED and PT are attached to the bottom disk. A wing attached to upper disk is set to mask 50% of the light flowing from the LED to PT. The PT outputs is proportional to the intensity of received light, i.e. measures directional displacement of gripper with respect to arm wrist. For each block, the sensors are set to uncouple horizontal displacement from vertical displacement. Each wing measures displacement in one direction and is large enough to eliminate the effect of displacement in the two other directions. This is shown on Figures 2-(c) and (d). This allows uncoupling the vertical displacement from a measured horizontal displacement.

FC was tested on the PUMA 560 robot arm using selective forces and torques and measurement of the corresponding sensor output. FC measures linear forces (up to ± 5 N) for small wing displacements of ± 1.5 mm within 10% errors.

A. Sensor kinematic model

The sensor consists of two solid and parallel disks (60mm D and 3mm thickness) that are linked by means of three cubic rubber blocks set at each of the above three directions. The robber blocks are attached to the disks at their contact bases. Since the wrist sensor is attached at the robot end, the robot end effector frame R_e is located at the center of one fixed disk and a compliant frame R_c is placed at the center of the other disk. Any external force applied to the tool causes a deflection represented by a translation and rotation of R_c with respect to R_e.

The sensors are placed at the left and right of each of the three rubber blocks denoted by A, B, and C. Each rubber block is surrounded by a left Xl and a right Xr sensing points, where X refers to rubber block A, B, or C. Since Xl is referenced in R_e, it is denoted by Xl_e. An external force and torque applied to tool, that is rigidly attached the R_C, causes: (1) translation of the origin of frame R_c by ΔX_e, and(2) a generalized rotation $M_{xyz}(\alpha, \beta, \gamma) = M_z M_y M_z$ of R_c with respect to R_e, where:

$$M_x(\alpha) = \begin{pmatrix} 1 & 0 & 0 \\ 0 & c\alpha & s\alpha \\ 0 & -s\alpha & c\alpha \end{pmatrix} \quad M_y(\beta) = \begin{pmatrix} c\beta & 0 & -s\beta \\ 0 & 1 & 0 \\ s\beta & 0 & c\beta \end{pmatrix}$$

$$M_z(\gamma) = \begin{pmatrix} c\gamma & -s\gamma & 0 \\ s\gamma & c\gamma & 0 \\ 0 & 0 & 1 \end{pmatrix} \quad (1)$$

The total differential of rotation matrix $M_{xyz}(\alpha, \beta, \gamma) = M_z M_y M_z$ is:

$$d(M_{xyz}(\alpha, \beta, \gamma)) = \frac{\partial M_x(\alpha)}{\partial \alpha} Myz(\beta, \gamma) d\alpha +$$

$$\frac{\partial M_y(\beta)}{\partial \beta} Mxz(\alpha, \gamma) d\beta + \frac{\partial M_z(\gamma)}{\partial \gamma} Mxy(\alpha, \beta) d\gamma \quad (2)$$

It can be easily shown that for small deflection angles α, β, and γ we have:

$$d(M_{xyz}(\alpha, \beta, \gamma)) = M_{\alpha, \beta, \gamma} = \begin{pmatrix} 0 & -\gamma & \beta \\ \gamma & 0 & -\alpha \\ \beta & \alpha & 0 \end{pmatrix} \quad (3)$$

Consider a sensing point X_e that is observed in R_e, we have:

$$O_e X_e = O_e O_c + M_{xyz}(\alpha, \beta, \gamma) O_c X_c \qquad (4)$$

where $O_e X_e$, $O_e O_c$, and $O_c X_c$ are the vectors of: (1) sensing point from the origin of R_e, (2) the origins of R_c from that of R_e, and (3) sensing point from the origin of R_c. Since an external force causes variation in the position ΔX_e and orientation $M_{\alpha,\beta,\gamma}$ of R_c, we have:

$$\Delta X_e = \Delta O_c + M(\alpha, \beta, \gamma) O_c X_c \qquad (5)$$

Where ΔX_e and $\Delta O_c = (\Delta x, \Delta y, \Delta z)^t$ are variations at the sensor location, at origin of R_c and $O_c X_c$ is known and fixed location of the sensing point observed in R_c. The problem is to compute translation ΔO_c of the compliance frame R_c and its elementary rotations α, β, and γ as function of sensor signal variations and location of sensing points. Specifically we have:

$$\Delta X_e = \begin{pmatrix} \Delta x \\ \Delta y \\ \Delta z \end{pmatrix} + \begin{pmatrix} 0 & -\gamma & \beta \\ \gamma & 0 & -\alpha \\ \beta & \alpha & 0 \end{pmatrix} O_c X_c \qquad (6)$$

Since each sensor can detect the motion of R_c in just one direction, thus only some components of ΔX_e are measurable. For example sensors located at Ar, Br and Cr detects translation of R_c plate only along the Z axis of R_e, i.e. the only measurable component of ΔAr_e is ΔAr_{ez}. For Bl, Al and Cl the measurable components are along the X axis of R_e, and the Y axis of R_e after rotating it by $\Pi/4$ and $-\Pi/4$, respectively.

Using Z components of equation 6, the sensors located at Ar, Br and Cr allow us to write:

$$\begin{pmatrix} \Delta Ar_{ez} \\ \Delta Br_{ez} \\ \Delta Cr_{ez} \end{pmatrix} = \begin{pmatrix} Ar_{cx} & Ar_{cy} & 1 \\ Br_{cx} & Br_{cy} & 1 \\ Cr_{cx} & Cr_{cy} & 1 \end{pmatrix} \begin{pmatrix} \beta \\ \alpha \\ \Delta O_{cz} \end{pmatrix} \qquad (7)$$

By inverting this matrix we find $(\beta, \alpha, \Delta O_{cz})^t = M^{-1}(\Delta Ar_{ez}, \Delta Br_{ez}, \Delta Cr_{ez})^t$.

Using the X component of equation 6, the sensor located at Bl measures Bl_{ex} which is a force component along the X axis of R_e. This allows us to write:

$$\Delta Bl_{ex} = \Delta x - \gamma \times Bl_{cy} + \beta \times Bl_{cz} \qquad (8)$$

Since Al and Cl are the measurable components along the Y axis of R_e after rotating R_e by $\Pi/4$ degrees and $-\Pi/4$, respectively. The implied change in the coordinate is represented by multiplying Equation 6 by the rotation matrix $M_y(\beta)$ given in Equation III-A, where β is $\Pi/4$ and $-\Pi/4$, respectively.

$$M_y(\beta)\Delta X_e = M_y(\beta) \begin{pmatrix} \Delta x \\ \Delta y \\ \Delta z \end{pmatrix} + \begin{pmatrix} 0 & -\gamma & \beta \\ \gamma & 0 & -\alpha \\ \beta & \alpha & 0 \end{pmatrix} O_c X_c \qquad (9)$$

Using the Y component of equation 9, the sensor located at Al (Cl) measures Al_{ey} (Cl_{ey}) a force component along the Y axis of R_e after affecting it by the above rotation matrices. Equation III-A and rotation matrix $M_y(\Pi/4)$ allow expressing the sensor data Al_{ey} as:

$$\Delta Al_{ey} = (c1 \times Al_{cx} + s1 \times Al_{cy})\Gamma - (s1 \times \beta + c1 \times \alpha)Al_{cz} - $$
$$s1 \times \Delta x + c1 \times \Delta y \qquad (10)$$

Similarly, Equation III-A and rotation matrix $M_y(-\Pi/4)$ allow expressing the sensor data Cl_{ey} as:

$$\Delta Cl_{ey} = (c2 \times Cl_{cx} + s2 \times Cl_{cy})\Gamma - (s2 \times \beta + c2 \times \alpha)Al_{cz} - $$
$$s2 \times \Delta x + c2 \times \Delta y \qquad (11)$$

Combining Equations 8, 10, and 11 we obtain:

$$\begin{pmatrix} \Delta Bl_{ex} - \beta \times Bl_{cz} \\ \Delta Al_{ey} + (s1 \times \beta + c1 \times \alpha)Al_{cz} \\ \Delta Cl_{ey} + (s2 \times \beta + c2 \times \alpha)Al_{cz} \end{pmatrix} = $$
$$\begin{pmatrix} -Bl_{cy} & 1 & 0 \\ c1 \times Al_{cx} + s1 \times Al_{cy} & -s1 & c1 \\ c2 \times Cl_{cx} + s2 \times Cl_{cy} & -s2 & c2 \end{pmatrix} \begin{pmatrix} \Gamma \\ \Delta x \\ \Delta y \end{pmatrix} \qquad (12)$$

Denote by U and M the vector and matrix that appear on the left hand side and right hand side of Equation 12, respectively. Thus $(\gamma, \Delta x, \Delta y) = M^{-1}V$, where ΔBl_{ex}, ΔAl_{ey}, and ΔCl_{ey} are the senor data, and all the other variables are either known or already determined from Equation 6. Therefore all the variational parameters as the translation $(\Delta x, \Delta y, \Delta z)$ and rotation (α, β, γ) are identified q based on reading of the six sensor data and known sensor locations.

IV. EVALUATION

We present a description of used system configuration, brief description of evaluated Internet delays to characterize the experiments, and a qualitative evaluation of contact forces in teleoperation.

A. System configuration

The client and server are run on PCs having 2-GHz Intel P4 processor with 1GB DRAM and 512 KB cache. Control of master and slave arms is done using Eagle PCI 30FG data acquisition cards. Each of client and server PCs is attached to a campus network by using a 100 Mbps NIC card (3com EtherLink XL PCI). The server PC is interfaced to two Sony Handycam digital cameras using a 400 mbps FireWire PCI (IEEE-1394) card. Both client and server PCs run under MS Window 2000 (ver. 5.00.2195) Paek 4. The server software uses MS Visual C++ with .NET framework 1.1 (ver. 1.1.4322) under Microsoft development environment 2003 (ver. 7.1.3088). The PUMA server is implemented using MS Visual C# with the above .NET framework. In the following experiments the operator uses a locally developed master arm, stereo vision (head-mounted display HMD) to appreciate the depth during tasks involving contact with the environment, and force feedback generated from the above force sensor. However, we only describe the interactions involving force feedback during some telerobotic tasks.
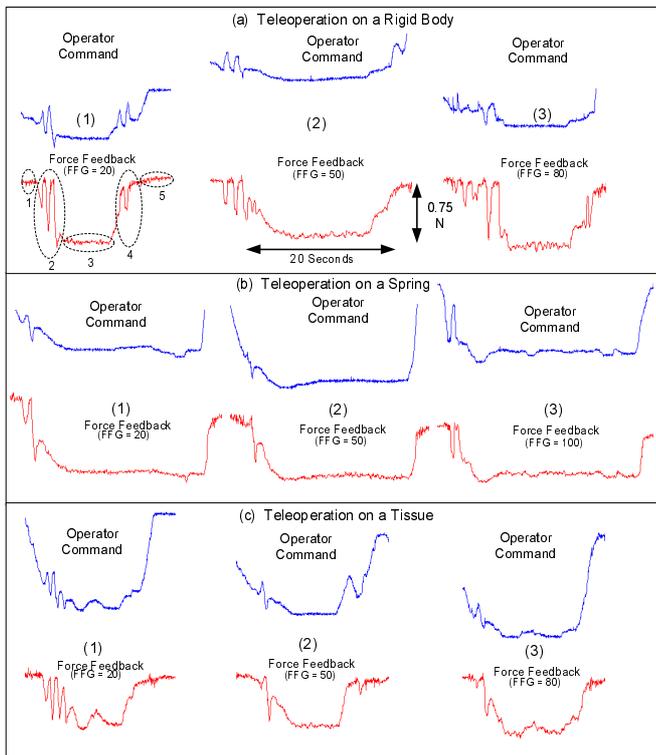
Fig. 3. Operator commands and force feedback during contact with a rigid body (a), a spring (b), and a tissue (c)

V. BRIEF RESULTS

Pipelining of grabbing stereo data with live transfer [7], [8] over the network allowed (1) copying a stereo frame from cameras to memory in 24 ms, and (2) live stereo video transfer at a rate of 17 fps. When network load is below 80%, the reference sampling rates for force feedback and operator command are 120 Hz and 50 Hz, respectively. The total delays for force and stereo are 8 ms and 83 ms, respectively. The slave arm is operated at a 10 Hz rate which leads to a round-trip delay of 183 ms or 5.5 Hz.

A. Bilateral teleoperation with force feedback

In direct teleoperation using reflected force feedback the user operate on the environment while minimizing contact forces. In this case a large control loop extending from the slave arm station to remote user is established including the user reaction time, the mechanical latencies, the network communication delays, and processing overhead. To shorten the loop a force regulation can be activated at the slave site to provide some active force compliance during direct teleoperation. In other words, coarse slave motion is controlled by the remote user and fine tool force control produces the needed tool compliance that minimizes contact force. In summary, the user leads the slave arm to contact the environment while the local controller corrects the tool positioning to minimize contact forces. The sampling frequency of the local compliance loop is about 5 Hz due to the mechanical delays of the PUMA slave arm. The master arm can display no more than 10 N force in any direction, i.e. a saturation effect is present beyond the above value. A visualization device is used to display to the operator the effective force applied to the hand through the master arm. The following contact experiments were carried out:

1) Contact with a rigid body. The user moves the slave arm to contact which create a contact force of 1N. The local compliance loop corrects the position of the slave tool to zero the external forces with a bouncing time of 2 s. Notice the oscillations (about 1 Hz) in force and their corresponding position which are caused by the rigid structure of object and the elasticity within the force sensor, i.e. between the slave arm wrist and the slave tool.
2) The contact with a rubber produces a contact force with a slower bouncing time (2 s) with slower oscillations of 0.75 Hz.
3) The contact with a spring produces a contact force with a slower bouncing time (3 s) but without oscillations.
4) The contact with a tissue produces a contact force with some histerisis due to loose contact when the contact force is about to be zeroed by the local compliance loop.

Figure 3 shows the force interaction during contact between the tool and (1) a rigid body (case a), (2) a spring (case b), and (3) a human muscle tissue (case c). Following the contact the operator was asked to maintain a force of 1 N on the target for 2 seconds. The tool force is shown on Figures 3-(a), (c), and and (e) and corresponding operator motion correction is shown on Figures 3-(b), (d), and (f), respectively. No force is displayed when the tool is in free space. Each contact has 5 phases which are (1) contact-free, (2) pre-contact, (3) contact, (4) pre-release, and (5) release. In both pre-contact and pre-release phases the teleoperation system is subject to vibrations which are displayed to the operator using a *force feedback gain* (FFG) which is intended to adjust the displayed force to a proper sensitivity level for the operator in connection with overall system stability. The operator feels the contact (wall effect) as well as the elasticity feature of some objects like the spring which was transmitted to the operator as a physical constraint on the master arm motion.

Figure 4 shows an extended pre-contact periods for each of the above cases and material. The reason for the vibration is that when the operator is starting the pre-contact phase the first contact leads to (1) a force feedback applied to master arm motor, (2) transmitting motor torques to operator through the dynamic of the linkage, and (3) producing a force bouncing (as the force feeling) from the operator hand back to the slave arm. This process continues to transmit contact forces from the scene and return a bouncing force from the operator until the elastic system between the target and operator hand is closed up by the operator engaging the slave closer and closer to target which amortize the above bouncing.

The bouncing is also partially caused by a force feedback that reaches the force display motors in the master arm to which the operator hand is linked through a wire-based transmission mechanism. Thus the motor reacts to the displayed force and its position sensor detect changes caused by above force. The client computer samples the master arm
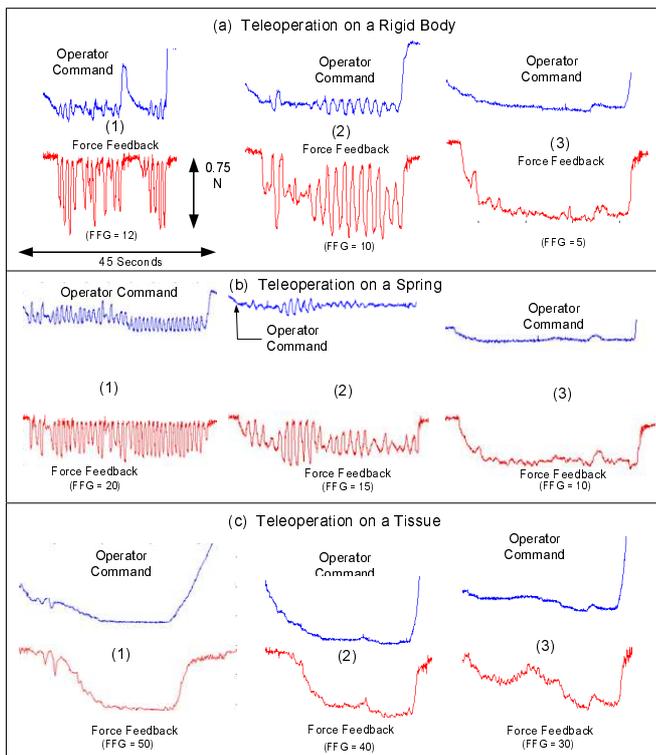
Fig. 4.   Extended command-force interactions of pre-contact for a rigid body (a), a spring (b), and a tissue (c)

position at its motors. Therefore, the client detect the reactive motion before this force is being transmitted to the operator. Therefore, it is imperative to use the least elastic transmission to partially reduce the above bouncing effects.

Note that the release phase is similar to the pre-contact phase. A high FFG gain may drive the telerobot out of control as shown in Figure 4-(a-1), (a-2), (b-1), and (b-2). Stable contact for the rigid and spring objects requires the use of lower FFG gains. The vibration frequency depends on: (1) stiffness of the target, (2) value of G, and (3) total round-trip delay of 183 ms. At the slave arm station, the rate of sensing-to-reaction or operator tool interaction is 5.5 Hz. Stiff targets produce prompt bouncing contact forces and therefore produce higher vibration frequency. The vibrations for rigid objects are greater and faster than those of the spring or the tissue. Contact forces transmitted from the scene return a bouncing force from the operator. This process continues until the contact is firmly engaged which amortize the above vibration. A high feedback gain may drive the telerobot out of control. Stable contact for the rigid and spring objects requires the use of moderate gains as compared to the case of the tissue. However, excessive gain values provides finer sensing but with the potential of unstable teleoperation.

The visco-elastic nature of the tissue makes it difficult to maintain a constant force contact. The tissue shape deformations causes instabilities even in the contact state, i.e. potential pre-contact in the middle of a contact phase. There are other important reasons for instability in Internet teleoperation which are due to transmission delays [9].

VI. CONCLUSION

A telerobotic system transmitting live motion commands, force feedback, and stereo video over the Internet is used to study the force feedback and operator interaction during contact with the environment. A parallel, 6 dof, compliant force sensor was presented. Kinematic analysis of the sensor mechanism allowed to compute the force applied the tool based on measurements made at the sensor tip. The force information is sampled and forwarded the client station where it is displayed on the operator hand. Evaluation is concerned with the process of moving the slave arm based on master arm motion, measuring force feedback at slave, forwarding the force data to master arm, display force data, and re-transmit operator motion. Interaction and force feedback generated during contact tasks were presented. Some bouncing oscillations were measured during pre-contact phases. Analysis shows that teleoperation network delays and transmission elasticity contribute to the instability of contact tasks. Modeling of the interaction for a given contact object is also needed to provide better teleoperation stability.

VII. ACKNOWLEDGEMENT

REFERENCES

[1] S.E. Salcudean, N.M. Wong, and R.L. Hollis. A force-reflecting teleoperation system with magnetically levitated master and wrist. *Proceedings of the IEEE International Conference on Robotics and Automation*, pages 1420–1426, 1992.
[2] S.E. Salcudean, N.M. Wong, and R.L. Hollis. Design and control of a force-reflecting teleoperation system with magnetically levitated master and wrist. *IEEE Transactions on Robotics and Automation*, 11(6):844–858, December 1995.
[3] P.J. Berkelman, L.L. Whitcomb, R.H. Taylor, and P. Jensen. A miniature microsurgical instrument tip force sensor for enhanced force feedback during robot-assisted manipulation. *IEEE Trans. on Robotics and Automation*, 19:5:917–921, Oct. 2003.
[4] L.E.P. Williams, R.B. Loftin, H.A. Aldridge, E.L. Leiss, and W.J. Bluethmann. Kinesthetic and visual force display for telerobotics. *IEEE Inter. Conf. on Robotics and Automation, ICRA '02*, 2:1249–1254, 2002.
[5] A. Codourey, M. Rodriguez, and I. Pappas. A task-oriented teleoperation system for assembly in the microworld. *Proc. 8th International Conference on Advanced Robotics, 1997. ICAR '97*, pages 235–240, July 1997.
[6] R.L. Kress, W.R. Hamel, P. Murray, and K. Bills. Control strategies for teleoperated Internet assembly. *IEEE/ASME Trans. on Mechatronics*, 6(4):410–416, Dec. 2001.
[7] M. Al-Mouhamed, O. Toker, and A. Iqbal. A multi-threaded distributed telerobotic framework. *IEEE Trans. on Mechatronics*, 11(5):558–566, October 2006.
[8] M. Al-Mouhamed, O. Toker, and A. Iqbal. Performance evaluation of a multi-threaded distributed telerobotic framework. *Submitted for publication*, December 2008.
[9] N. Funabiki, K. Morishige, and H. Noborio. Sensor-based motion-planning of a manipulator to overcome large transmission delays in teleoperation. *Proc. IEEE Int. Conf. on Systems, Man, and Cybernetics, 1999. IEEE SMC '99*, 5:1117–1122, Oct. 1999.